PAPER

Check for updates

Highly twisted bipolar molecules for efficient near-ultraviolet organic light-emitting diodes *via* a hybridized local and charge-transfer mechanism†

Ziting Zhong,‡[a] Zhangshan Liu,‡[b] Sinuo Geng,[a] Huihui Li,[a] Xin Jiang Feng, [iD] *[a] Zujin Zhao [iD] *[b] and Hua Lu [iD] *[a]

Near ultraviolet (NUV) electroluminescence (EL) is very important but seldom reported for being short of short-wavelength emitters. Herein, we report two highly twisted terphenyl-based donor−acceptor molecules exhibiting excellent thermal and morphological stability and nearly quantitative NUV luminescence. *Via* a hybridized local and charge-transfer (HLCT) process, excellent NUV EL is achieved with a maximum external quantum efficiency of 6.97% and CIE$_{x,y}$ of (0.16, 0.06) in a nondoped OLED. The device shows excellent colour purity with a small full width at half maximum of 48 nm. Our research demonstrates that highly twisted structures can efficiently tune the luminescence wavelength of bipolar molecules to the NUV region and achieve high-performance NUV EL.

Introduction

Near ultraviolet (NUV) organic light-emitting diodes (OLEDs) have attracted extensive attention for their potential applications.[1–9] However, NUV OLEDs with good performances are very limited due to the scarcity of luminescent emitters with emission peaks around 400 nm and Commission Internationale de L'Eclairage (CIE) coordinate *y* values of less than 0.06.[10–22] Usually, NUV emissions are achieved by emitters with short conjugation and low molecular weight. Unfortunately, short-conjugation molecules often show weak luminescence and low carrier transport ability, while molecules with low molecular weights exhibit inferior thermal and morphological stabilities.[23,24] These factors are detrimental to preparing high-performance OLED devices. As a result, design of emitters for efficient NUV OLEDs is a considerable challenge.[25–33] On the other hand, the exciton utility of luminescent molecules is a significant factor for electroluminescence efficiency. For the reason of achieving theoretically the full

use of excitons, thermally activated delayed fluorescence (TADF) emitters are widely used.[34–41] TADF materials often exhibit a severe intramolecular charge transfer (ICT) effect and seldom emit NUV light. Furthermore, efficiency roll-off in TADF emitter-based OLEDs is also a common problem due to their long-delayed lifetime.[37] Fluorescent emitters with hybridized local and charge-transfer (HLCT) excited states, also coined as the "hot exciton" mechanism, can make full use of the excitons theoretically *via* reverse intersystem crossing (RISC) from high-lying triplet states (T_n, $n > 1$) to singlet states and have aroused extensive interest.[38–42] From the view of electronic structure, HLCT emitters should meet the requirements of a large $\Delta E(T_n \leftrightarrow T_1)$ and a small $\Delta E(T_n \leftrightarrow S_m)$, where $n \geq 2$ and $m \geq 1$.[43] Considering the PL spectra, the CT energy level of HLCT molecules decreases with an increase in the solvent polarity due to the solvatochromic effect, by which the CT and LE levels can be evaluated.[44] HLCT molecules radiate *via* a locally excited (LE)-emissive state, preventing long-wavelength shift, and exhibit small efficiency roll-off by rapid RISC.[45–47] By modulating the LE and CT states in molecules, several NUV OLEDs have been fabricated based on HLCT molecules.[6,48–55] Nevertheless, highly efficient and stable NUV OLEDs are still being urgently developed.

HLCT-featured molecules usually exhibit low to moderate luminescence with longer wavelengths due to the CT state, leading to the lack of NUV luminogens.[55] Increasing the twisting angles in the donor/acceptor (D/A) group by incorporating steric groups is an appealing method for weakening the electronic and intermolecular interaction.[55–59] In this work, large hindrance groups dimethylphenylsilyl- and methyldiphenylsilyl- were used to reduce the electronic D/A conjugation and π−π stacking in the

[a] *College of Material Chemistry and Chemical Engineering, Key Laboratory of Organosilicon Chemistry and Material Technology, Ministry of Education, Key Laboratory of Organosilicon Material Technology, Zhejiang Province, Hangzhou Normal University, Hangzhou, 311121, Zhejiang, People's Republic of China. E-mail: xjfeng@hznu.edu.cn, hualu@hznu.edu.cn; Tel: +86 (0) 571-28867825*

[b] *Center for Aggregation-Induced Emission, State Key Laboratory of Luminescent Materials and Devices, South China University of Technology, Guangzhou, 510640, China. E-mail: mszjzhao@scut.edu.cn*

† Electronic supplementary information (ESI) available: Experimental details, additional spectroscopic properties, NMR spectra and HRMS spectra. See DOI: https://doi.org/10.1039/d2tc04421h

‡ These authors contributed equally to this work.

This journal is © The Royal Society of Chemistry 2023

J. Mater. Chem. C, 2023, **11**, 1733–1741 | **1733**

phenanthroimidazole (PI) derivatives. As expected, a highly twisted structure is conducive to achieving NUV emission with nearly quantitative fluorescence quantum yields and high thermal/morphological stability. The nondoped OLEDs radiate NUV light (Commission Internationale de L'Eclairage (CIE) coordinates of (0.161, 0.063) for **C2MPI** and (0.162, 0.058) for **C2PPI** as emitters) with emission maxima of 404 and 406 nm, respectively. The maximum external quantum efficiencies (EQE$_{max}$) are as high as 6.97% and 5.55% for devices using **C2MPI** and **C2PPI** as emitters, respectively.

Results and discussion

Synthesis

Target molecules and their preparation methods are outlined in Scheme 1. Compounds **3** and **4** were obtained by lithiation and substitution with the corresponding chlorosilane followed by palladium-catalyzed amination. Intermediate **6** was synthesized by boration of compound **5** which was obtained by Debus–Radziszewski imidazole synthesis from phenanthrene-9,10-dione. *Via* palladium-catalyzed Suzuki-Miyaura coupling with compound **6** and compound **3** or **4**, **C2MPI** and **C2PPI** were prepared and characterized by ^{1}H NMR, ^{13}C NMR, and HRMS.

Thermal and photophysical properties

High decomposition temperatures (T_d) of 463 and 481 °C were achieved for **C2MPI** and **C2PPI**, respectively. The transition temperature (T_g) for **C2MPI** was 110 °C, while there was no T_g detected for **C2PPI** (Fig. S1, inset, ESI†). These results indicate
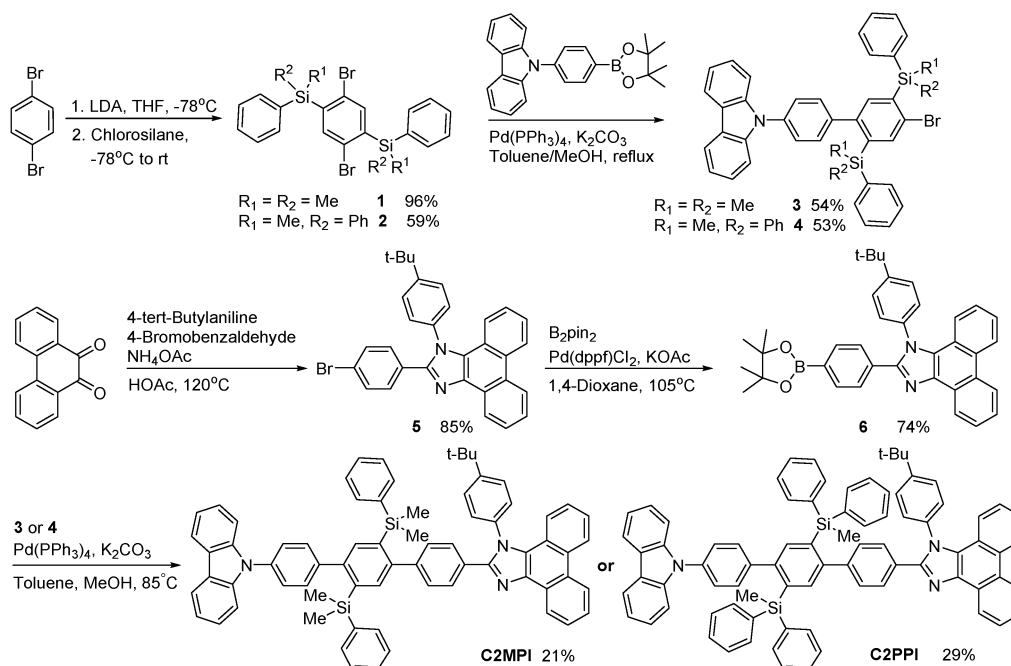
Table 1 Photophysical, thermal and morphological measurements of **C2MPI** and **C2PPI**

	λ_{abs}[a] (nm)	ε_{abs}[b] (M cm^{-1})	λ_{em}[c] (nm)	$\Delta\nu_{em\text{-}abs}$[d] (cm^{-1})	Φ_F[e]	τ_F[f] (ns)	T_g/T_d[g] (°C)
C2MPI	328	48 400	402/425	5612	0.86/0.99	1.63/1.69	110/463
C2PPI	330	69 000	410/425	5913	0.90/0.99	1.44/1.02	nd/481

[a] Absorption maxima in toluene. [b] Molar extinction coefficient. [c] Emission maxima in toluene and in neat films. [d] Stokes shift. [e] Absolute fluorescence quantum yields in toluene/neat films. [f] τ_F is PL lifetime in toluene/doped films. [g] Glass transition and decomposition temperatures. nd = not detected.

that the thermal/morphological stabilities of the molecules are good for solid emission.

The photophysical properties were investigated and are shown in Table 1, Tables S1 and S2 (ESI†). The absorption and emission spectra in different solvents are shown in Fig. 1a and b, Fig. S2 and S3 (ESI†). The bands around 330 to 341 nm are ascribed to S$_0$ → S$_1$ transitions of molecules. The weak peaks around 364 nm should be associated with the CT transition.[49,60] The absorption spectra are affected little by solvent polarity, which indicates that the chromophores possess small dipole moments in the ground states (Fig. S2 and Table S1, ESI†). Comparatively small solvatochromism of emission with 19 and 21 nm was found from nonpolar to polar solvents for **C2MPI** and **C2PPI**, respectively, which indicates small dipole moments for the two dyes in the excited states (Fig. S3, ESI†). The dyes exhibit very high fluorescence quantum efficiencies as high as 0.99 and there is no obvious concentration quenching with the increase of emitters in films with sharper emission spectra as compared to those in solutions (Fig. 1a, b and Fig. S4, ESI†). Short lifetimes at the nano-level

Scheme 1 Synthetic routes and molecule structures of **C2MPI** and **C2PPI**.

1734 | *J. Mater. Chem. C*, 2023, **11**, 1733–1741

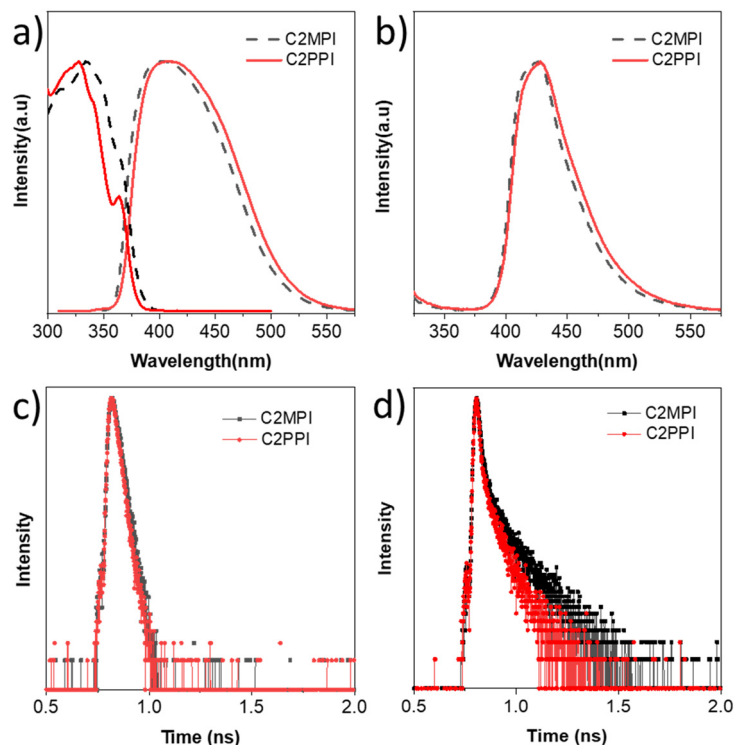This journal is © The Royal Society of Chemistry 2023

Fig. 1 (a) Absorption and emission spectra in toluene. (b) Emission in neat films. (c) Transient PL spectra of **C2MPI** and **C2PPI** in toluene and (d) Transient PL spectra of **C2MPI** and **C2PPI** in neat films.

were detected, exhibiting single-component characteristics. (Fig. 1c and d). These results infer that these materials are potential candidates for device application.

Electrochemical nature and calculation study

The electrochemical properties of **C2MPI** and **C2PPI** were investigated by cyclic voltammetry (CV) performed in 0.1 M Bu_4NPF_6 dichloromethane. **C2MPI** and **C2PPI** exhibit irreversible one-electron oxidation/reduction waves with an E_{onset} of $0.80/-2.61$ and $0.79/-2.58$ eV *versus* Fc/Fc^+ (0.13 V), respectively. By $E_{HOMO/LUMO} = -(4.8\ eV + E_{onset})$, the HOMOs/LUMOs are calculated to be $-5.60/-2.19$ and $-5.59/-2.22$ eV for **C2MPI** and **C2PPI**, respectively. From the absorption spectra, the optical energy gaps (E_gs) were estimated as 3.25 and 3.22 eV for **C2MPI** and **C2PPI**, respectively (Fig. 2 and Table 2). As a result, the LUMOs for **C2MPI** and **C2PPI**, determined from $E_g = E_{HOMO} - E_{LUMO}$, are -2.35 and -2.33 eV, respectively, and they are very close to those calculated from reductive potentials in CV. Apparently, the HOMOs, LUMOs and E_gs of **C2MPI** are very close to those of **C2PPI**.

Information on molecular orbitals (MO) was obtained by DFT with Gaussian16 package by B3LYP/6-31G(d,p).[61] Fig. 3a shows the molecular configurations and the frontier MO as well as their energy levels. **C2MPI** and **C2PPI** exhibit localized HOMOs on the imidazole ring and the conjugated aryls. However, the tertiary-butyl substituted phenyl ring almost makes no contribution to MO due to its poor conjugation with the imidazole centre. The dyes show delocalized LUMOs distributed in the conjugation
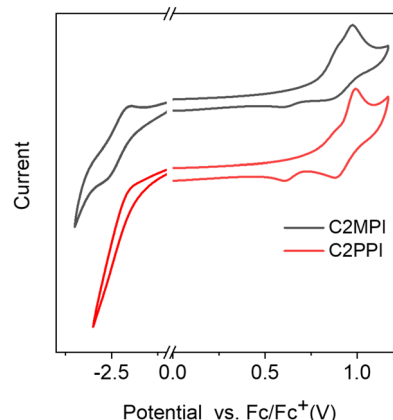

Fig. 2 Cyclic voltammograms of **C2MPI** and **C2PPI**, measured in *N,N*-dimethylformamide (negative) and in dichloromethane (positive) containing tetra-*n*-butylammonium hexafluorophosphate (0.1 M) at a scan rate of 50 mV s^{-1}.

bridge backbone and the imidazole ring. Obviously, the silyl groups on the terphenyl disrupt the conjugation between carbazolyl and PI and affect the electron distribution. The electron distributions reveal that the lowest transitions of these molecules are mainly associated with the HOMO to LUMO transitions, which was manifested by the TD-DFT calculation (Table S3, ESI†). The charge distribution with a large HOMO–LUMO overlap reveals that **C2MPI** and **C2PPI** exhibit LE-dominated HLCT character, which matches the solvent effects well. Twisting angles of

This journal is © The Royal Society of Chemistry 2023

J. Mater. Chem. C, 2023, **11**, 1733–1741 | **1735**

Table 2 Electrochemical properties and energy gaps of **C2MPI** and **C2PPI**

	E_{onset}^{oxd} (V)[a]	E_{onset}^{red} (V)[a]	HOMO[b] (eV)	LUMO (eV)	E_g (eV)	θ_1^d (°)	θ_2^d (°)	HOMO[d] (eV)	LUMO[d] (eV)	E_g^e (eV)
C2MPI	0.80	−2.61	−5.60	$-2.19^b/-2.35^c$	$3.41^b/3.25^c$	61.65	68.40	−5.19	−1.18	4.01
C2PPI	0.79	−2.58	−5.59	$-2.22^b/-2.37^c$	$3.37^b/3.22^c$	61.62	59.23	−5.15	−1.22	3.83

[a] E_{onset} vs Fc/Fc⁺. [b] Estimated by CV measurements calculated with $E_{HOMO/LUMO} = -(4.8 + E_{onset})$ eV and $E_g = E_{LUMO} - E_{HOMO}$. [c] Optical energy gap determined by the absorption cutoff and LUMO calculated by $E_g^{opt} = E_{LUMO} - E_{HOMO}$. [d] Calculated by the optimized structures in DFT calculations, and θ_1 and θ_2 mean the twist angles between the benzyl rings in the terphenyl linker. [e] $E_g^{opt} = E_{LUMO} - E_{HOMO}$.
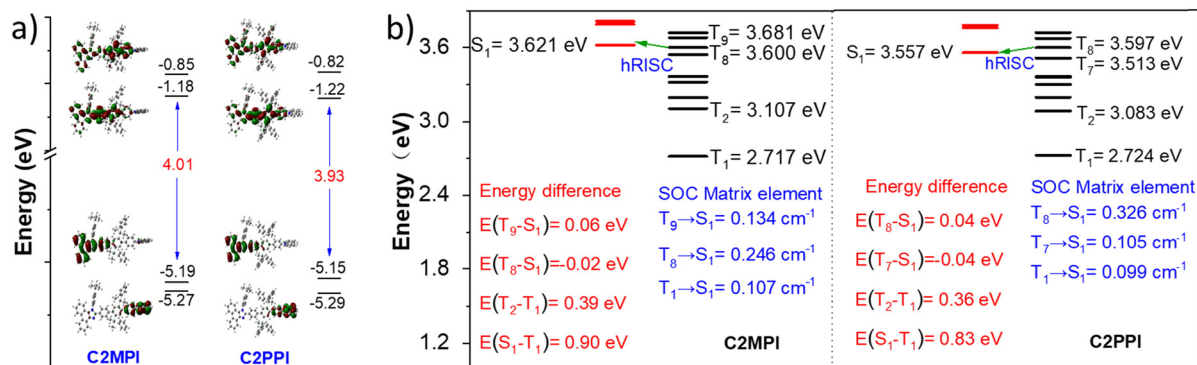

Fig. 3 (a) Configuration and frontier molecular orbital diagrams for **C2MPI** and **C2PPI** by B3LYP/6-31G(d,p). (b) Singlet/triplet energy levels and SOC matrix elements of **C2MPI** and **C2PPI** in the gas phase, calculated by the TD-DFT method from optimized S_1 geometries. (Section 2.3).

59–68° were found in the terphenyls, indicating that these molecules have a more twisted linker compared to the molecules unsubstituted or with less steric substituents (Fig. S5, ESI†).[62,63] Such torsions can influence the electronic structures in the molecules and keep the molecules from close stacking in the solid states. The large energy gaps (E_gs), calculated from HOMOs–LUMOs or by CV and absorption cutoffs, are favourable for NUV emission (Table 2).

The pathway of exciton utility was studied by TD-DFT calculations by B3LYP/6-31G(d,p) basic sets and their excited states were investigated (Fig. 3b). The splitting energy between the singlet and triplet energy levels (ΔE_{S1-T1}) is 0.90 and 0.83 eV for **C2MPI** and **C2PPI**, respectively. Generally, a small ΔE_{S1-T1} (<0.1 eV) is required to achieve an efficient TADF process. Therefore, the TADF process is unfavourable for both materials. Considerable spin–orbit coupling (SOC) was found between S_1 and T_{7-9}. Therefore, the high performances for the non-doped devices can be ascribed to hRISC of excitons.[55,64,65] The natural transition orbital (NTO) calculations also indicate that the $S_0 \rightarrow S_1$ transition displays LE-dominated HLCT characteristics with a large overlap of "hole" and "particle" for **C2MPI** and **C2PPI**. The "hole" is dispersed on the molecular backbone and a "particle" is located on the linker and imidazole ring. Balanced CT/LE components were found in S_1 and T_{7-9} and this is beneficial for achieving hRISC and radiative transition from S_1 to S_0 during electroluminescence in devices (Fig. S6, ESI†).[66,67]

Electroluminescence performance

Non-doped OLEDs were fabricated using **C2MPI** and **C2PPI** as emitters with a configuration of ITO/HATCN (5 nm)/TAPC (X nm)/TCTA (5 nm)/Emitter (20 nm)/TPBi (40 nm)/LiF (1 nm)/Al (Device B1, Emitter = **C2MPI**, X = 60; Device B5, Emitter = **C2PPI**, X = 50). HATCN (1,4,5,8,9,11-hexaazatriphenylenehexacarbonitrile), TAPC (bis(di-4-tolylaminophenyl)cyclohexane), TCTA (tris(4-carbazoyl-9-ylphenyl)amine) and TPBi (1,3,5-tris(N-phenylbenzimidazol-2-yl)benzene) are used as hole injection, hole-transporting, electron-blocking, and electron-transporting layers, respectively (Fig. 4).

$$\eta_{ext} = \gamma \times \eta_{PL} \times \eta_r \times \eta_{out} \tag{1}$$

The EL profiles are shown in Fig. 5 and the device performances are listed in Table 3. Devices B1 and B5 emit NUV lights close to the blue index (0.15, 0.06) with $CIE_{x,y}$ of (0.161, 0.063)
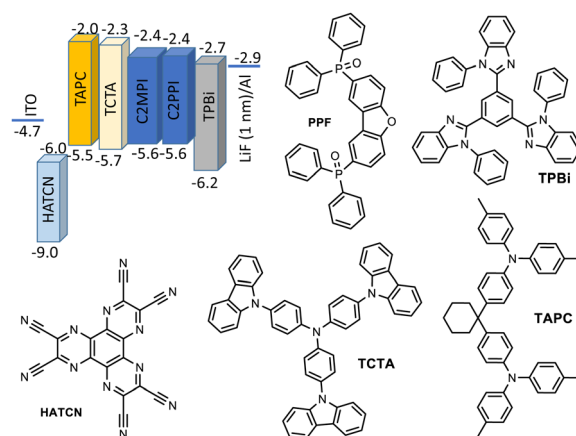

Fig. 4 Nondoped device configuration, molecules used and their energy levels.

1736 | *J. Mater. Chem. C*, 2023, **11**, 1733–1741

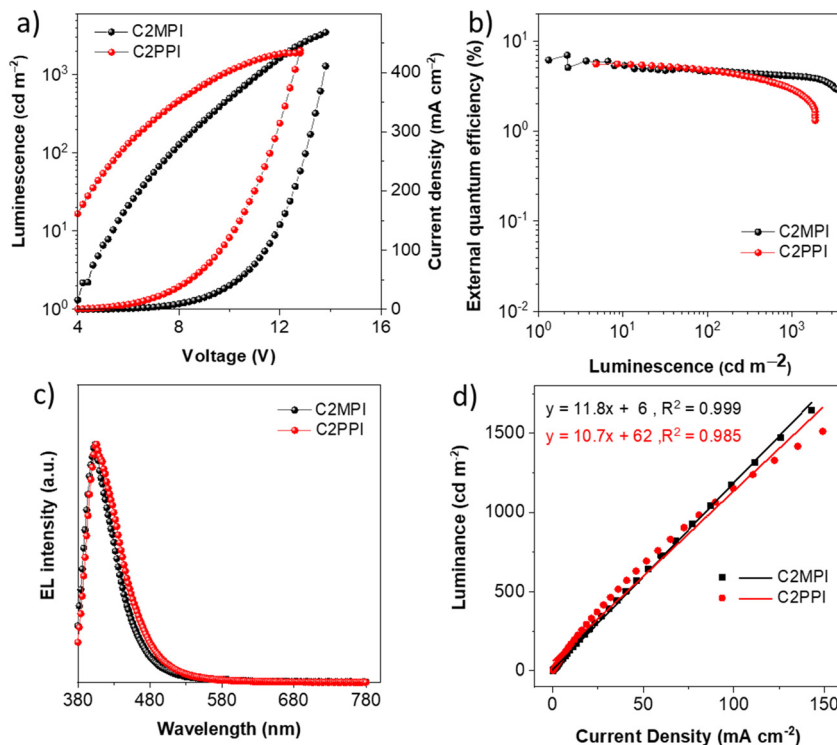This journal is © The Royal Society of Chemistry 2023

Fig. 5 Device configuration (a) Luminance–voltage–current density characteristics. (b) External quantum efficiency–luminance characteristics. (c) EL spectra. (d) Luminance *versus* current density (symbol) and the fitted curve plot (line) of devices.

and (0.162, 0.058) for **C2MPI** and **C2PPI**, respectively. Their devices show emission maxima at 404 nm (**C2MPI**) and 406 nm (**C2PPI**) with low turn-on voltages of 3.9 and 3.3 V for **C2MPI** and **C2PPI**, respectively. Impressively, narrow EL spectra with small FWHMs of 48 nm and 54 nm are observed at 3.9 V for device B1 and 3.3 V for device B5, respectively, showing that the devices exhibit excellent colour purity (Fig. 5). Moreover, the nondoped devices exhibit merely short-wavelength emission, which indicates that the excitons recombine completely within the emitting-layer and the radiation derives from the singlet excitons only. The device efficiencies are tabulated in Table 3. Devices B1 and B5 exhibit excellent EL performances and the EQEs are larger than 5%. Note that device B1 has a very high maximum EQE of 6.97% and a maximum exciton utility efficiency (EUE) of

35% calculated by eqn (1), in which γ is the balance factor of carriers (100%), η_{PL} is the neat-film fluorescence efficiency (99%) for **C2MPI**, and η_{out} stands for the light extraction rate (20%).[68] The EUE of device B1 significantly exceeds 25%, which indicates the utility of triplet excitons. To explore the mechanism of exciton utility, plots of luminance *versus* current density were made and good linearity is observed, excluding the triplet–triplet annihilation process. Meanwhile, large energy gaps between S_1 and T_1 of **C2MPI** (0.90 eV) and **C2PPI** (0.83 eV) are observed (Fig. 3b), indicating that the TADF process is not favoured (usually energy splitting is less than 100 mV between S_1 and T_1 for the TADF process).[69] So, devices B1 and B5 exhibit excellent performances *via* an HLCT process, which is also supported by the calculation of excited energy levels and SOC.

Table 3 EL results of **C2MPI** and **C2PPI** in devices

Emitter	Device	$\lambda_{EL}{}^a$ (nm)	Fwhm^b (nm)	V^c (V)	L^d (cd m^{-2})	$\eta_C{}^d$ (cd A^{-1}) Maximum value/at 100 cd m^{-2}	$\eta_P{}^d$ (lm W^{-1})	$\eta_{ext}{}^d$ (%)	CIE^e (x, y)
C2MPI	**B1**	404	48	3.9	3500	1.75/1.34	1.20/0.55	6.97/4.57	(0.161,0.063)
	B2	388	nd	4.9	681	0.60/0.59	0.24/0.20	1.96/1.93	(0.189,0.114)
	B3	396	nd	4.9	795	0.69/0.68	0.25/0.24	2.60/2.57	(0.184,0.099)
	B4	396	nd	4.5	1042	0.87/0.84	0.33/0.31	3.30/3.20	(0.179,0.086)
C2PPI	**B5**	406	54	3.3	1900	1.83/1.57	1.69/0.88	5.55/4.76	(0.162,0.058)
	B6	406	56	3.3	1877	1.67/1.51	1.53/0.84	4.20/3.79	(0.165,0.067)
	B7	406	54	3.3	2057	1.78/1.64	1.62/0.89	4.63/4.27	(0.166,0.065)
	B8	406	53	3.3	2274	1.90/1.76	1.73/0.95	4.98/4.61	(0.166,0.064)

^{a} Emission maxima. ^{b} Full width at half maximum (nd, the spectra are not intact because light <380 nm cannot be collected.). ^{c} Turn-on voltage at 1 cd m^{-2}. ^{d} The luminescence (L), current efficiency (η_c), power efficiency (η_P) and external quantum efficiency (η_{ext}) of the devices: maximum values/values at 100 cd m^{-2}. ^{e} CIE coordinates at 100 cd m^{-2}.

This journal is © The Royal Society of Chemistry 2023

J. Mater. Chem. C, 2023, **11**, 1733–1741 | **1737**

Doped devices were fabricated using 5–20% **C2MPI** as the emitter and 2,8-bis(diphenylphosphoryl)dibenzo[*b,d*]furan (PPF) as the host and device B1 exhibited superior efficiency and colour purity to devices B2–B4. (Fig. S7–S10, ESI,† Table 3). Besides, changing the electron-transporting layer or adding additional carrier blocking layers in the devices doesn't help to improve the efficiencies using **C2PPI** as the emitter (devices B6–B8). These results indicated that functional layers with more appropriate HOMO/LUMO alignments are needed to achieve better device performances in future work (Fig. S7–S10, ESI,† Table 3).

Conclusions

In this study, two highly twisted D–A molecules, carbazolyl and phenanthroimidazole end-capped with terphenyls, were designed and synthesized. The chromophores show good thermal and morphological stabilities. The dyes emitted NUV light in nonpolar solvents and in the solid states. Nondoped OLEDs were prepared and good EL efficiencies were achieved due to the utility of the triplet excitons *via* the HLCT process. The non-doped OLED, fabricated with **C2MPI** as the emitting-layer, radiates NUV light peaking at 404 nm with $CIE_{x,y}$ of (0.161, 0.063) and a small FWHM of 48 nm. The device also showed a very high maximum EQE of 6.97%. DFT and TD-DFT calculations combined with photophysical investigation revealed the HLCT characteristic of these dyes and the high EUE was derived from the conversion of high-lying triplet excitons in the excited states. This study manifests that twisted terphenyl conjugated D–A molecules can be used as emitters to achieve high performance NUV OLEDs.

Experimental section

Synthesis. Compound 1. To a solution of 1,4-dibromobenze (1.3 g, 5.5 mmol), and chlorodimethylphenylsilane (2.0 mL, 12 mmol) in THF (20 mL), lithium diisopropylamide (6.0 mL, 2 M) was added at −78 °C under nitrogen. The resultant mixture was stirred for 1 h at −78 °C and then allowed to warm to room temperature. Upon completion, 20 mL of water was added to the reactants and the mixture was extracted with ethyl acetate (20 mL × 2). The combined ethyl acetate was washed with brine (20 mL), dried over sodium sulphate and evaporated to give an oil. This residue was purified to give 2.7 g of compound **1** in 96% yield. ^{1}H NMR (400 MHz, CDCl$_3$) δ 7.53–7.51 (m, 4H), 7.43 (s, 2H), 7.41–7.34 (m, 6H), 0.65 (s, 12H). ^{13}C NMR (100 MHz, CDCl$_3$) δ 143.27, 141.01, 136.43, 134.22, 129.37, 127.88, −2.06. HR-MS: Calcd. For $C_{24}H_{24}Br_2Si_2$ [M + H]$^+$ 502.9783. Found 502.9799.

Compound 2. Using 1,4-dibromobenze (2.6 g, 11.0 mmol), chlorodiphenylmethylsilane (5.6 g, 22.0 mmol), lithium diisopropylamide (12.0 mL, 2.0 M), and THF (20 mL), 4.0 g of compound **2** was prepared in 59% yield by the same method reported for compound **1**. ^{1}H NMR (400 MHz, CDCl$_3$) δ 7.51–7.49 (m, 8H), 7.42–7.37 (m, 10H), 7.36–7.35 (m, 2H), 7.28 (s, 2H), 0.97 (s, 6H). ^{13}C NMR (100 MHz, CDCl$_3$) δ 142.61, 142.31, 135.17, 134.62, 129.96, 128.00, −3.15. HR-MS: Calcd. For $C_{34}H_{28}Br_2Si_2$ [M + H]$^+$ 627.0096. Found 627.0105.

Compound 3. A solution of compound **1** (2.7 g, 5.4 mmol), 9*H*-carbazole, 9-[4-(4,4,5,5-tetramethyl-1,3,2-dioxaborolan-2-yl)phenyl]- (1.0 g, 2.7 mmol), potassium carbonate (0.3 g, 2.2 mmol), and tetrakis(triphenylphosphine)palladium (0.2 g, 0.14 mmol) in toluene (40 mL) and methanol (10 mL) was heated to 85 °C and stirred overnight under nitrogen. The reaction mixture was cooled and washed with H$_2$O and brine. The organic phase was collected, dried, and evaporated to a residue, which was columned to give compound **3** (0.85 g, 54%) as a white solid. ^{1}H NMR (400 MHz, CDCl$_3$) δ 8.09 (d, *J* = 8.0 Hz, 2H), 7.76 (s, 1H), 7.36 (m, 2H), 7.31–7.28 (m, 11H), 7.25–7.21 (m, 4H), 7.11 (d, *J* = 8.4 Hz, 2H), 0.64 (s, 6H), 0.26 (s, 6H). ^{13}C NMR (100 MHz, CDCl$_3$) δ 148.02, 143.99, 141.05, 139.85, 138.75, 138.30, 137.59, 136.36, 134.36, 134.02, 132.52, 131.14, 130.97, 129.36, 128.98, 128.04, 127.90, 126.36, 126.29, 126.06, 123.16, 120.46, 119.22, 109.95, −0.90, −2.28. HR-MS: Calcd. For $C_{40}H_{36}BrNSi_2$ [M + H]$^+$ 666.1570. Found 666.1580.

Compound 4. Using compound **2** (4.0 g, 5.4 mmol), 9*H*-carbazole, 9-[4-(4,4,5,5-tetramethyl-1,3,2-dioxaborolan-2-yl)phenyl]- (1.0 g, 2.7 mmol), potassium carbonate (0.3 g, 2.2 mmol), tetrakis(triphenylphosphine)palladium (0.25 g, 0.22 mmol), toluene (40 mL) and methanol (10 mL), 1.0 g of compound **4** was prepared in 47% yield by the same method reported for compound **3**. ^{1}H NMR (400 MHz, CDCl$_3$) δ 8.16 (d, *J* = 7.6 Hz, 2H), 7.65–7.59 (m, 5H), 7.47–7.26 (m, 26H), 7.14 (d, *J* = 8.4 Hz, 1H), 1.04 (s, 2H), 0.90 (s, 1H), 0.40 (s, 3H). ^{13}C NMR (100 MHz, CDCl$_3$) δ 146.86, 140.84, 140.72, 139.65, 138.94, 137.77, 136.11, 135.85, 135.35, 135.15, 135.10, 131.08, 130.86, 129.54, 129.24, 128.05, 127.97, 127.90, 126.11, 125.92, 123.40, 120.35, 12.00, 119.93, −2.39, −2.84. HR-MS: Calcd. For $C_{50}H_{40}BrNSi_2$ [M + H]$^+$ 790.1883. Found 790.1895.

Compound 5. A mixture of 9,10-phenanthrenedione (2.1 g, 10.0 mmol), 4-tertbutylaniline (4.50 g, 0.05 mol), *p*-bromobenzaldehyde (1.90 g, 10 mmol), ammonium acetate (3.10 g, 40.0 mmol) and acetic acid (150 mL) was added into a round-bottomed flask and degassed with nitrogen. The reaction was stirred under reflux for 24 h. The mixture was cooled to rt and filtered to give a white solid. The solid was washed with H$_2$O (80 mL) and 25 mL of methanol to afford 4.0 g of compound **5** as white powder in 67% yield. ^{1}H NMR (400 MHz, CDCl$_3$) δ 8.85 (d, *J* = 6.8 Hz, 1H), 8.76 (d, *J* = 8.4 Hz, 1H), 8.70 (d, *J* = 8.4 Hz, 1H), 7.75–7.42 (m, 1H), 7.67–7.65 (m, 1H), 7.61 (d, *J* = 8.4 Hz, 2H), 7.53–7.49 (m, 1H), 7.47–7.45 (m, 2H), 7.42–7.40 (m, 4H), 7.19 (dd, *J* = 8.4, 0.8 Hz, 1H), 1.46 (s, 9H).

Compound 6. A mixture of compound **5** (5.1 g, 10.0 mmol), bis(pinacolato)diboron (3.0 g, 12.0 mmol), potassium acetate (3.0 g, 30.0 mmol), Pd(dppf)Cl$_2$ (0.2 g, 3.0 mmol) and dry dioxane (50 mL) was refluxed under nitrogen for 24 h. The reaction mixture was cooled to room temperature and filtered to give a grey solid, which was purified to give 4.1 g of compound **6** as a white solid in 74% yield. ^{1}H NMR (400 MHz, CDCl$_3$) δ 8.79 (d, *J* = 8.0 Hz, 1H), 8.66 (d, *J* = 8.4 Hz, 1H), 8.61 (d, *J* = 8.4 Hz, 1H), 7.63 (m, 3H), 7.55–7.48 (m, 5H), 7.42–7.38 (m, 1H), 7.32 (d, *J* = 8.0 Hz, 2H), 7.18–7.14 (m, 2H), 7.06 (d, *J* = 8.0 Hz, 1H), 1.36 (s, 9H), 1.25 (s, 12H).

C2MPI. A solution of compound **6** (1.8 g, 3.3 mmol), compound **3** (0.7 g, 1.1 mmol), Pd(PPh$_3$)$_4$ (0.1 g, 0.1 mmol), aq.

1738 | *J. Mater. Chem. C*, 2023, **11**, 1733–1741

This journal is © The Royal Society of Chemistry 2023

K$_2$CO$_3$ (0.5 mL, 2 M), toluene (50 mL) and methanol (10 mL) were stirred at 85 °C overnight under nitrogen. Upon completion, a filtrate was obtained by filtration, which was evaporated to afford a grey residue. The residue was columned and recrystallized to afford 234 mg of **C2MPI** as a white solid in 21% yield. ^{1}H NMR (400 MHz, CD$_2$Cl$_2$) δ 8.61 (d, J = 8.4 Hz, 2H), 8.56 (d, J = 8.4 Hz, 1H), 7.97 (d, J = 7.6 Hz, 2H), 7.59–7.55 (m, 1H), 7.49–7.47 (m, 3H), 7.43 (s, 1H), 7.40 (s, 1H), 7.32–7.26 (m, 5H), 7.25–7.21 (m, 8H), 7.17–7.09 (m, 14H), 6.90 (d, J = 8.0 Hz, 2H), 1.26 (s, 9H), 0.15 (s, 6H), 0.00 (s, 6H). ^{13}C NMR (100 MHz, CD$_2$Cl$_2$) δ 153.75, 150.73, 148.36, 146.87, 144.77, 143.50, 141.26, 139.96, 138.05, 138.00, 136.99, 136.88, 136.12, 134.30, 134.21, 131.84, 129.71, 129.45, 129.24, 128.99, 128.57, 128.11, 127.70, 127.47, 126.73, 126.55, 126.35 125.90, 125.30, 124.41, 123.68, 123.60, 122.88, 121.41, 120.62, 120.31, 111.38, 34.89, 29.53, −0.45. HR-MS: Calcd. For C$_{71}$H$_{62}$N$_3$Si$_2$ [M + H]$^+$ 1012.4486. Found 1012.4477.

C2PPI. The same procedure for **C2MPI** was used using compound **6** (2.5 g, 2.0 mmol), compound **4** (1.2 g, 0.6 mmol), Pd(PPh$_3$)$_4$ (0.2 g, 0.06 mmol), aq. K$_2$CO$_3$ (0.3 mL, 2 M), toluene (50 mL) and methanol (10 mL) to obtain 198 mg **C2PPI** as a white solid in 29% yield. ^{1}H NMR (400 MHz, CD$_2$Cl$_2$) δ 8.81 (d, J = 8.3 Hz, 2H), 8.76 (d, J = 8.1 Hz, 1H), 8.16 (d, J = 7.7 Hz, 2H), 7.78 (m, 1H), 7.68 (d, J = 8.5 Hz, 3H), 7.54–7.28 (m, 40H), 7.21 (d, J = 8.3 Hz, 2H), 6.98 (d, J = 8.0 Hz, 2H), 1.48 (s, 9H), 0.45 (s, 3H), 0.15 (s, 3H). ^{13}C NMR (100 MHz, CDCl$_3$) δ 153.74, 147.35, 147.14, 143.12, 141.13, 139.07, 138.96, 137.73, 137.56, 136.85 136.70, 136.54, 135.49, 135.42, 130.95, 129.66, 129.63, 129.58, 129.42, 129.08, 128.92, 128.54, 128.25, 128.23, 127.67, 127.44, 126.70, 126.44, 125.15, 124.39, 123.58, 122.83, 121.37, 120.56, 120.28, 110.29, 34.74, 26.51, −2.52, −3.16. HR-MS: Calcd. For C$_{81}$H$_{66}$N$_3$Si$_2$ [M + H]$^+$ 1136.4786. Found 1136.4790.

Spectroscopic measurements, Device fabrication and DFT calculations are displayed in the ESI.†

Author contributions

Z. Z. and Z. L. contributed equally to this work. All the authors were involved in the analysis and interpretation of data. Z. Zhong did the synthesis work, characterized the photophysical properties, and analyzed part of the data. Z. Liu fabricated the devices, did the EL measurements and analyzed the data. S. Geng and H. Li did part of the photophysical and thermal measurements. X. J. Feng prepared the original draft and wrote the manuscript. Z. Zhao prepared the original draft and wrote the manuscript. H. Lu prepared the original draft and wrote the manuscript.

Conflicts of interest

There are no conflicts to declare.

Acknowledgements

References

1 X. Lv, M. Sun, L. Xu, R. Wang, H. Zhou, Y. Pan, S. Zhang, Q. Sun, S. Xue and W. Yang, *Chem. Sci.*, 2020, **11**, 5058–5065.
2 Y. Liu, H. Liu, Q. Bai, C. Du, A. Shang, D. Jiang, X. Tang and P. Lu, *ACS Appl. Mater. Interfaces*, 2020, **12**, 16715–16725.
3 S. Yang, Y. Zhang, A. Khan, Y.-J. Yu, S. Kumar, Z.-Q. Jiang and L.-S. Liao, *J. Mater. Chem. C*, 2020, **8**, 3079–3807.
4 H. Zhang, J. Zeng, W. Luo, H. Wu, C. Zeng, K. Zhang, W. Feng, Z. Wang, Z. Zhao and B. Z. Tang, *J. Mater. Chem. C*, 2019, **7**, 6359–6368.
5 X. Qiu, S. Ying, C. Wang, M. Hanif, Y. Xu, Y. Li, R. Zhao, D. Hu, D. Ma and Y. Ma, *J. Mater. Chem. C*, 2019, **7**, 592–600.
6 T.-C. Chao, Y.-T. Lin, C.-Y. Yang, T. S. Hung, H.-C. Chou, C.-C. Wu and K.-T. Wong, *Adv. Mater.*, 2005, **17**, 992–996.
7 J. Lin, X. Guo, Y. Lv, X. Liu and Y. Wang, *ACS Appl. Mater. Interfaces*, 2020, **12**, 10717.
8 H. van Santen and J. H. M. Neijzen, *Jpn. J. Appl. Phys.*, 2003, **42**, 1110–1112.
9 J. Shinar and R. Shinar, *J. Phys. D: Appl. Phys.*, 2008, **41**, 133001.
10 S. Y. Lee, T. Yasuda, Y. S. Yang, Q. Zhang and C. Adachi, *Angew. Chem., Int. Ed.*, 2014, **53**, 6402–6406.
11 C.-C. Peng, S.-Y. Yang, H.-C. Li, G.-H. Xie, L.-S. Cui, S.-N. Zou, C. Poriel, Z.-Q. Jiang and L.-S. Liao, *Adv. Mater.*, 2020, **32**, 2003885.
12 X. Chen, D. Ma, T. Liu, Z. Chen, Z. Yang, J. Zhao, Z. Yang, Y. Zhang and Z. Chi, *CCS Chem.*, 2021, **4**, 1284–1294.
13 J. Chen, J. Zeng, X. Zhu, J. Guo, Z. Zhao and B. Z. Tang, *CCS Chem.*, 2020, **3**, 230–240.
14 Y. Xu, X. Liang, X. Zhou, P. Yuan, J. Zhou, C. Wang, B. Li, D. Hu, X. Qiao, X. Jiang, L. Liu, S.-J. Su, D. Ma and Y. Ma, *Adv. Mater.*, 2019, **31**, 1807388.
15 X. Guo, P. Yuan, J. Fan, X. Qiao, D. Yang, Y. Dai, Q. Sun, A. Qin, B. Z. Tang and D. Ma, *Adv. Mater.*, 2021, **33**, 2006953.
16 S.-N. Zou, X. Chen, S.-Y. Yang, S. Kumar, Y.-K. Qu, Y.-J. Yu, M.-K. Fung, Z.-Q. Jiang and L.-S. Liao, *Adv. Opt. Mater.*, 2020, **8**, 2001074.
17 C. Brouillac, W.-S. Shen, J. Rault-Berthelot, O. Jeannin, C. Quinton, Z.-Q. Jiang and C. Poriel, *Mater. Chem. Front.*, 2022, **6**, 1803–1813.
18 A. Monkman, *ACS Appl. Mater. Interfaces*, 2022, **14**, 20463–20467.
19 C. Poriel, J. Rault-Berthelot and Z.-Q. Jiang, *Mater. Chem. Front.*, 2022, **6**, 1246–1252.
20 J.-H. Lee, C.-H. Chen, P.-H. Lee, H.-Y. Lin, M.-K. Leung, T.-L. Chiu and C.-F. Lin, *J. Mater. Chem. C*, 2019, **7**, 5874–5888.
21 C. Poriel and J. Rault-Berthelot, *Adv. Funct. Mater.*, 2020, **30**, 1910040.
22 Y. Wang, J. H. Yun, L. Wang and J. Y. Lee, *Adv. Funct. Mater.*, 2020, **31**, 2008332.

This journal is © The Royal Society of Chemistry 2023

J. Mater. Chem. C, 2023, **11**, 1733–1741 | 1739

23 X. Tang, L. Yao, H. Liu, F. Shen, S. Zhang, Y. Zhang, H. Zhang, P. Lu and Y. Ma, *J. Mater. Chem. C*, 2014, **2**, 5019–5027.

24 H. Liu, Q. Bai, L. Yao, H. Zhang, H. Xu, S. Zhang, W. Li, Y. Gao, J. Li, P. Lu, H. Wang, B. Yang and Y. Ma, *Chem. Sci.*, 2015, **6**, 3797–3804.

25 H. Zhang, G. Li, X. Guo, K. Zhang, B. Zhang, X. Guo, Y. Li, J. Fan, Z. Wang, D. Ma and B. Z. Tang, *Angew. Chem., Int. Ed.*, 2021, **60**, 22241–22247.

26 Y. Luo, S. Li, Y. Zhao, C. Li, Z. Pang, Y. Huang, M. Yang, L. Zhou, X. Zheng, X. Pu and Z. Lu, *Adv. Mater.*, 2020, **32**, 2001248.

27 M. Chen, Y. Liao, Y. Lin, T. Xu, W. Lan, B. Wei, Y. Yuan, D. Li and X. Zhang, *J. Mater. Chem. C*, 2020, **8**, 14665–14694.

28 J. Tagare, R. A. K. Yadav, S. S. Swayamprabha, D. K. Dubey, J.-H. Jou and S. Vaidyanathan, *J. Mater. Chem. C*, 2021, **9**, 4935–4947.

29 J. Tagare, R. Boddula, S. S. Sudheendran, D. K. Dubey, J.-H. Jou, S. Patel and S. Vaidyanathan, *J. Mater. Chem. C*, 2020, **8**, 16834–16844.

30 Y. Yang, P. Cohn, S.-H. Eom, K. A. Abboud, R. K. Castellano and J. Xue, *J. Mater. Chem. C*, 2013, **1**, 2867.

31 C. Lin, P. Han, S. Xiao, F. Qu, J. Yao, X. Qiao, D. Yang, Y. Dai, Q. Sun, D. Hu, A. Qin, Y. Ma, B. Z. Tang and D. Ma, *Adv. Funct. Mater.*, 2021, **31**, 2106912.

32 F.-C. Kong, Y.-L. Zhang, C. Quinton, N. McIntosh, S.-Y. Yang, J. Rault-Berthelot, F. Lucas, C. Brouillac, O. Jeannin, J. Cornil, Z.-Q. Jiang, L.-S. Liao and C. Poriel, *Angew. Chem., Int. Ed.*, 2022, **61**, e202207204.

33 Q. Wang, F. Lucas, C. Quinton, Y.-K. Qu, J. Rault-Berthelot, O. Jeannin, S.-Y. Yang, F.-C. Kong, S. Kumar, L.-S. Liao, C. Poriel and Z.-Q. Jiang, *Chem. Sci.*, 2020, **11**, 4887–4894.

34 H. Uoyama, K. Goushi, K. Shizu, H. Nomura and C. Adachi, *Nature*, 2012, **492**, 234–238.

35 J. Wei, C. Zhang, D. Zhang, Y. Zhang, Z. Liu, Z. Li, G. Yu and L. Duan, *Angew. Chem., Int. Ed.*, 2021, **60**, 12269–12273.

36 Q. Zhang, J. Li, K. Shizu, S. Huang, S. Hirata, H. Miyazaki and C. Adachi, *J. Am. Chem. Soc.*, 2012, **134**, 14706–14709.

37 S. Xue, X. Qiu, S. Ying, Y. Lu, Y. Pan, Q. Sun, C. Gu and W. Yang, *Adv. Opt. Mater.*, 2017, **5**, 1700747.

38 W. Li, D. Liu, F. Shen, D. Ma, Z. Wang, T. Feng, Y. Xu, B. Yang and Y. Ma, *Adv. Funct. Mater.*, 2012, **22**, 2797–2803.

39 X. He, J. Lou, B. Li, H. Wang, X. Peng, G. Li, L. Liu, Y. Huang, N. Zheng, L. Xing, Y. Huo, D. Yang, D. Ma, Z. Zhao, Z. Wang and B. Z. Tang, *Angew. Chem., Int. Ed.*, 2022, **61**, e202209425.

40 W. J. Chung, K. H. Lee, M. Jung, K. M. Lee, H. C. Park, M.-S. Eum and J. Y. Lee, *Adv. Opt. Mater.*, 2021, **9**, 2100203.

41 S.-Y. Yang, Z.-Q. Feng, Z. Fu, K. Zhang, S. Chen, Y.-J. Yu, B. Zou, K. Wang, L.-S. Liao and Z.-Q. Jiang, *Angew. Chem., Int. Ed.*, 2022, **61**, e202206861.

42 S. Hirata, Y. Sakai, K. Masui, H. Tanaka, S. Y. Lee, H. Nomura, N. Nakamura, M. Yasumatsu, H. Nakanotani, Q. Zhang, K. Shizu, H. Miyazaki and C. Adachi, *Nat. Mater.*, 2015, **14**, 330–336.

43 Y. Pan, W. Li, S. Zhang, L. Yao, C. Gu, H. Xu, B. Yang and Y. Ma, *Adv. Opt. Mater.*, 2014, **2**, 510–515.

44 W. Li, Y. Pan, L. Yao, H. Liu, S. Zhang, C. Wang, F. Shen, P. Lu, B. Yang and Y. Ma, *Adv. Opt. Mater.*, 2014, **2**, 892–901.

45 Y. Liu, L. Yang, Q. Bai, W. Li, Y. Zhang, Y. Fu and F. Ye, *Chem. Eng. J.*, 2021, **420**, 129939.

46 S. Yang, Y. Zhang, F. Kong, Y. Yu, H. Li, S. Zou, A. Khan, Z. Jiang and L. Liao, *Chem. Eng. J.*, 2021, **418**, 129366.

47 H. Zhang, J. Zeng, W. Luo, H. Wu, C. Zeng, K. Zhang, W. Feng, Z. Wang, Z. Zhao and B. Z. Tang, *J. Mater. Chem. C*, 2019, **7**, 6359–6368.

48 X. Tang, L. Yao, H. Liu, F. Shen, S. Zhang, Y. Zhang, H. Zhang, P. Lu and Y. Ma, *J. Mater. Chem. C*, 2014, **2**, 5019–5027.

49 H. Liu, Q. Bai, L. Yao, H. Zhang, H. Xu, S. Zhang, W. Li, Y. Gao, J. Li, P. Lu, H. Wang, B. Yang and Y. Ma, *Chem. Sci.*, 2015, **6**, 3797–3804.

50 Z.-Q. Wang, C.-L. Liu, C.-J. Zheng, W.-Z. Wang, C. Xu, M. Zhu, B.-M. Ji, F. Li and X.-H. Zhang, *Org. Electron.*, 2015, **23**, 179–185.

51 S. Xiao, Y. Gao, R. Wang, H. Liu, W. Li, C. Zhou, S. Xue, S. Zhang, B. Yang and Y. Ma, *Chem. Eng. J.*, 2022, **440**, 135911.

52 H. L. Lee, W. J. Chung and J. Y. Lee, *Small*, 2020, **16**, 1907569.

53 S. Chen, C. Zhang and H. Xu, *Chem. Eng. J.*, 2021, **429**, 132327.

54 Y. Chen, N. Li, Z. Huang, G. Xie and C. Yang, *Chem. Eng. J.*, 2022, **430**, 133078.

55 J. Chen, H. Liu, J. Guo, J. Wang, N. Qiu, S. Xiao, J. Chi, D. Yang, D. Ma, Z. Zhao and B. Z. Tang, *Angew. Chem., Int. Ed.*, 2022, **61**, e202116810.

56 Y. Zheng, Z. Wang, X. Wang, J. Li, X. J. Feng, G. He, Z. Zhao and H. Lu, *ACS Appl. Electron. Mater.*, 2021, **3**, 422–429.

57 Y. Zheng, X. Zhu, Z. Ni, X. Wang, Z. Zhong, X. J. Feng, Z. Zhao and H. Lu, *Adv. Opt. Mater.*, 2021, **9**, 2100965.

58 Z. Zhong, X. Zhu, X. Wang, Y. Zheng, S. Geng, Z. Zhou, X. J. Feng, Z. Zhao and H. Lu, *Adv. Funct. Mater.*, 2022, **32**, 2112969.

59 X. Xiang, Z. Zhou, H. Feng, S. Feng, L. Gai, H. Lu and Z. Guo, *CCS Chem.*, 2020, **2**, 329–336.

60 Y. Zhang, S.-L. Lai, Q.-X. Tong, M.-F. Lo, T.-W. Ng, M.-Y. Chan, Z.-C. Wen, J. He, K.-S. Jeff, X.-L. Tang, W.-M. Liu, C.-C. Ko, P.-F. Wang and C.-S. Lee, *Chem. Mater.*, 2012, **24**, 61–70.

61 M. J. Frisch, G. W. Trucks, H. B. Schlegel, G. E. Scuseria, M. A. Robb, J. R. Cheeseman, G. Scalmani, V. Barone, B. Mennucci, G. A. Petersson, H. Nakatsuji, M. Caricato, X. Li, H. P. Hratchian, A. F. Izmaylov, J. Bloino, G. Zheng, J. L. Sonnenberg, M. Hada, M. Ehara, K. Toyota, R. Fukuda, J. Hasegawa, M. Ishida, T. Nakajima, Y. Honda, O. Kitao, H. Nakai, T. Vreven, J. A. Montgomery, J. E. Peralta Jr., F. Ogliaro; M. Bearpark, J. J. Heyd, E. Brothers, K. N. Kudin, V. N. Staroverov, T. Keith, R. Kobayashi, J. Normand, K. Raghavachari, A. Rendell, J. C. Burant, S. S. Iyengar, J. Tomasi, M. Cossi, N. Rega, J. M. Millam, M. Klene, J. E. Knox, J. B. Cross, V. Bakken, C. Adamo, J. Jaramillo, R. Gomperts, R. E. Stratmann, O. Yazyev, A. J. Austin, R. Cammi, C. Pomelli, J. W. Chterski, R. L. Martin,

1740 | *J. Mater. Chem. C*, 2023, **11**, 1733–1741

This journal is © The Royal Society of Chemistry 2023

K. Morokuma, V. G. Zakrzewski, G. A. Voth, P. Salvador, J. J. Dannenberg, S. Dapprich, A. D. Daniels, O. Farkas, J. B. Foresman, J. V. Ortiz, J. Cioslowski and D. J. Fox, *Gaussian 16, Revision C.01*, Gaussian, Inc., Wallingford CT, 2016.

62 X. Ouyang, X.-L. Li, L. Ai, D. Mi, Z. Ge and S.-J. Su, *ACS Appl. Mater. Interfaces*, 2015, **7**, 7869–7877.

63 J. Huang, J.-H. Su, X. Li, M.-K. Lam, K.-M. Fung, H.-H. Fan, K.-W. Cheah, C. H. Chen and H. Tian, *J. Mater. Chem.*, 2011, **21**, 2957.

64 O. R. Meitei, S. E. Houck and N. Mayhall, *J. Chem. Theory Comput.*, 2020, **16**, 3597–3606.

65 Q. Zhu, S. Feng, X. Guo, X. Chen and J. Zhang, *Spectrochim. Acta, Part A*, 2019, **221**, 117214.

66 R. L. Martin, *J. Chem. Phys.*, 2003, **118**, 4775–4777.

67 Y. Sagara, K. Shizu, H. Tanaka, H. Miyazaki, K. Goushi, H. Kaji and C. Adachi, *Chem. Lett.*, 2014, **44**, 360–362.

68 L. J. Rothberg and A. J. Lovinger, *J. Mater. Res.*, 1996, **11**, 3174–3187.

69 N. A. Kukhta, T. Matulaitis, D. Volyniuk, K. Ivaniuk, P. Turyk, P. Stakhira, J. V. Grazulevicius and A. P. Monkman, *J. Phys. Chem. Lett.*, 2017, **8**, 6199–6205.

This journal is © The Royal Society of Chemistry 2023

J. Mater. Chem. C, 2023, **11**, 1733–1741 | **1741**